JASMAC Conference of the Japan Society of Microgravity Application

P13

音響場で浮遊する多成分液滴の蒸発に伴う自然乳化・相分離

Emulsification and phase separation associated with evaporation of multicomponent droplets in acoustic levitation

○光野海祥 [1]，長谷川浩司 [2]
○**Misaki MITSUNO[1], Koji HASEGAWA[2]**
[1] 工学院大学大学院工学研究科機械工学専攻，Graduate School of Engineering, Kogakuin University
[2] 工学院大学工学部機械工学科，Department of Mechanical Engineering, Kogakuin University

1. Introduction

In recent years, contactless sample manipulation technology in midair has been attracting great attention in the fields of biochemistry and pharmaceutical science. One of the promising methods is the acoustic levitation [1)]. This method enables us to levitate, transport, mix, and evaporation of samples in resonant acoustic fields [2)]. The acoustic levitation method is also expected to be applied in microgravity environments, where it can levitate larger sample with lower acoustic pressure than that in 1G [3)]. However, it has been pointed out that this method causes nonlinear and dynamic behaviors such as unsteady translational motion [4)] and evaporation behavior [5)] in the levitated sample. Although there are many previous studies on the evaporation behavior of one or two component droplets, experimental studies on the evaporation behavior of three or more component droplets are still in the development stage. In this study, we aim to understand the evaporation dynamics of spontaneous emulsification and phase separation of Ouzo droplets [6)] premixed with water, ethanol and anise oil upon evaporation. To achieve this, the spontaneous emulsification and phase separation process of Ouzo droplets upon evaporation was visualized and analyzed using a droplet evaporation model.

2. Experimental method

Figure 1 (a) shows a schematic diagram of the experimental setup used in this study. A sinusoidal signal generated by a function generator is input to the ultrasonic transducer. The ultrasonic wave is emitted from the tip of the lower horn connected to the ultrasonic transducer and is reflected by the upper reflector to form an acoustic standing wave between the horn and the reflector as shown in **Figure 1 (b)**. A liquid droplet is injected using a syringe near the acoustic pressure node of the acoustic standing wave to levitate a droplet. A high-speed camera and IR camera are used to capture the droplet motion using the backlight method and the surface temperature of levitated droplets. The obtained images are processed using a computer and in-house code.

The reflector shape used in this experiment has a radius of curvature of 36 mm (R36). The frequency is 19.3 kHz and the wavelength λ is 18 mm. The width of the horn and reflector is 36 mm ($\approx 2\lambda$). The distance between the horn and reflector is 48 mm ($\approx 5\lambda/2$). The ambient temperature is 23±2°C and the humidity is 55 ±5%.

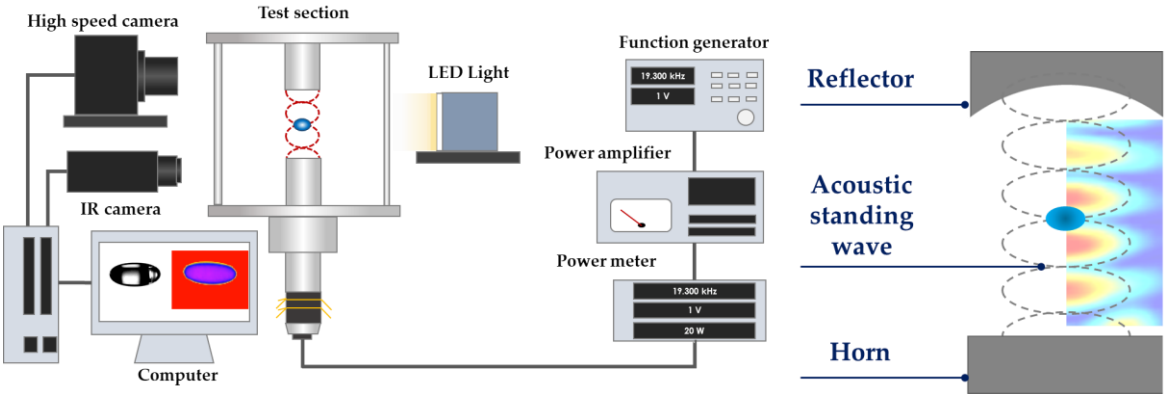

(a) (b)

Figure 1 Schematic of acoustic levitator: (a) experimental setup and (b) levitation principle.

3. Results and discussions

Figure 2 (a) shows the time series of Ouzo droplets with the ethanol concentration of 70%. **Figure 2 (b)** shows the evaporation process of Ouzo droplets. The left and right vertical axes represent normalized surface area $(d/d_0)^2$ and aspect ratio, respectively. d and d_0 are the instantaneous and the initial droplet diameter. The highlighted area in **Fig. 2 (b)** indicates the time at which each droplet observed the Ouzo effect. From the results, $(d/d_0)^2$ decreased by approximately 50% in 200 seconds. With respect to the Ouzo effect, we confirmed that each droplet emulsified for 20 to 30 seconds. When comparing the droplet diameter and aspect ratio, both sets of experimental data demonstrated similar decreasing trends. The aspect ratio asymptotically approached a spherical shape as the droplets evaporated.

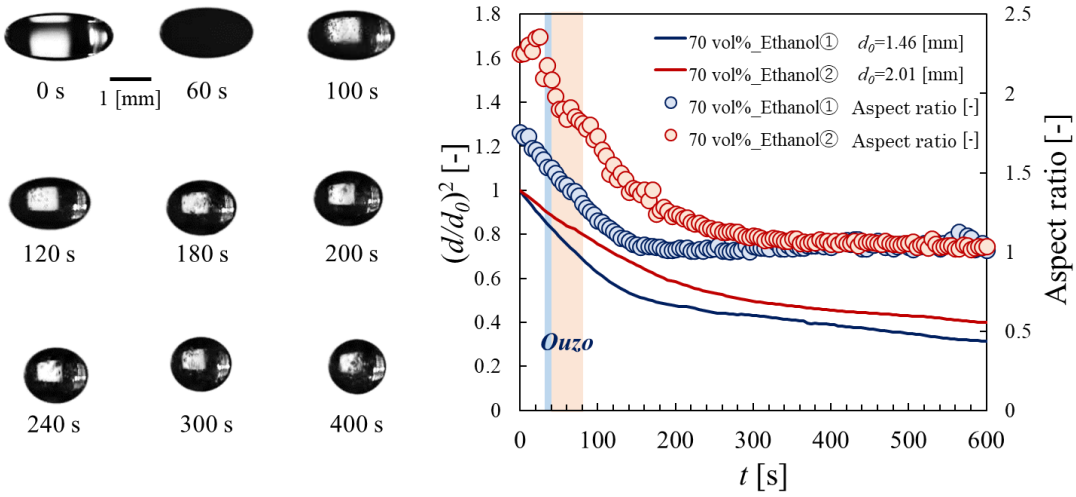

(a) Snapshot of Ouzo droplet during evaporation (b) Time evolution of $(d/d_0)^2$ and *As*

Figure 2 Evaporation process of Ouzo droplets (ethanol: 70 vol%, water: 29 vol%, anise oil: 1 vol%).

Figure 3 (a) shows the evaporation process for ethanol concentrations of 50%, 70%, and 90%, with the diameter on the vertical axis. In contrast, **Figure 3 (b)** shows a normalized result with $(d/d_0)^2$ for the vertical axis and the Fourier number for the horizontal axis. The Fourier number can be expressed by the following equation.

$$Fo = \frac{Dt}{{d_0}^2} \tag{1}$$

where t is time and D is the diffusion coefficient. The diffusion coefficient of ethanol was used in the present study. These results illustrate a gradual change in droplet size during the evaporation depending on the ethanol concentration. Notably, **Figure 3 (b)** shows the experimental data for evaporating droplets with the same concentration converged when using nondimensional values.

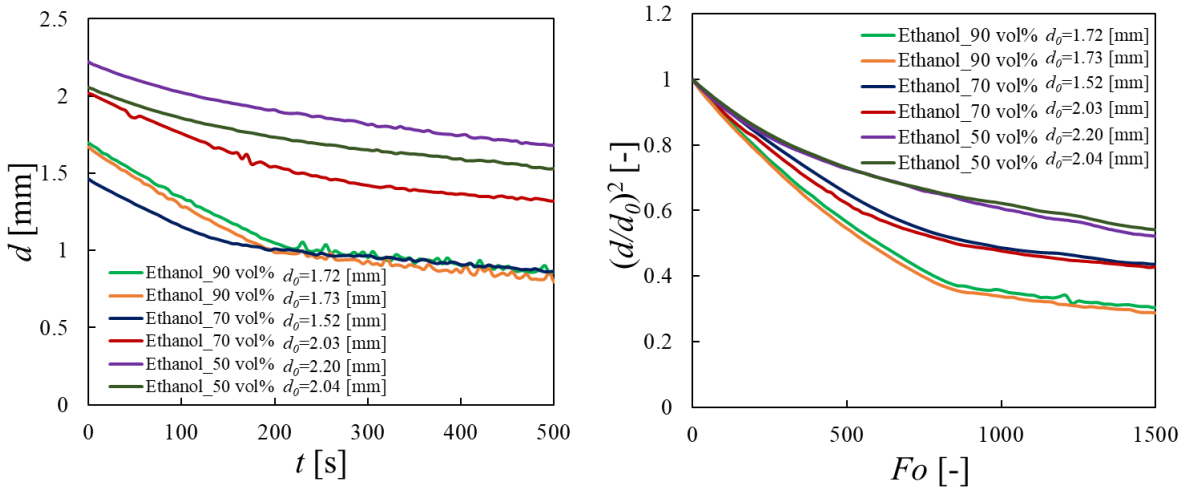

(a) dimensional form (b) non-dimensional form

Figure 3 Evaporation process of Ouzo droplets for different concentration.

Figure 4 shows the start/end time (Ouzo time) and duration time of the Ouzo effect. **Figure 4 (a)** shows the effect of the ethanol concentration on Ouzo time. The start time was defined as the moment the emulsification appeared in the droplet, and the end time was when it disappeared, as observed through visualization. **Figure 4 (b)** shows the the effect of the ethanol concentration on the duration time of the Ouzo effect. These results represent that the Ouzo effect occurred during droplet levitation when the ethanol concentration was between 40% and 90%. We also confirmed that the higher ethanol concentration delayed the onset time and shortened the duration of the Ouzo effect.

These results indicate that there are four distinct phases of evaporation of levitated ouzo droplets illustrated in **Figure 5**: 1) preferential evaporation of ethanol, 2) onset of the Ouzo effect, 3) generation of core-shell structure due to evaporation of ethanol component, and 4) Remaining presence of only oil droplets due to evaporation of water component. These findings can facilitate our understanding of evaporation and phase separation for levitated ternary droplets, paving the way for contactless droplet manipulation. For a deeper understanding of the evaporation and phase separation process, the instantaneous concentration condition for the Ouzo effect needs to be explored based on the experimental results and evaporation model.

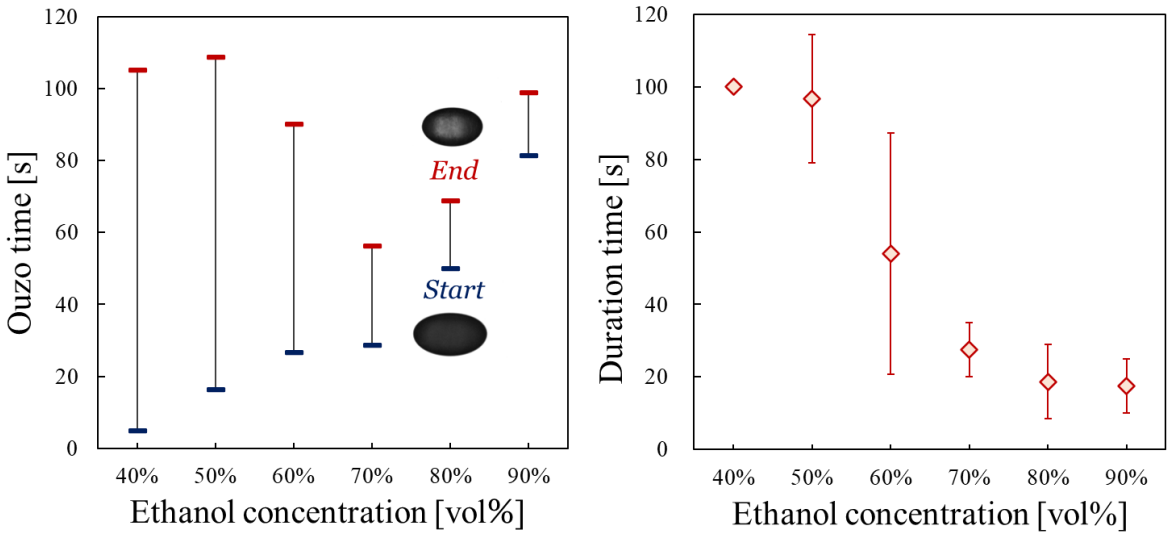

(a) Start and end time of Ouzo effect (anise oil: 1 vol%)

(b) Duration time of Ouzo effect

Figure 4 Characteristic time of Ouzo effect associated with evaporation.

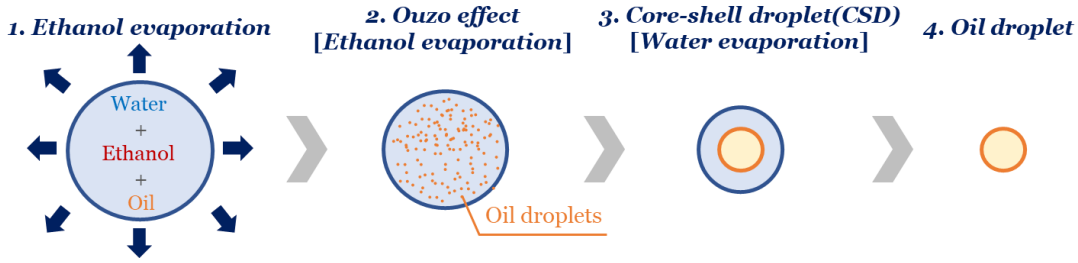

Figure 5 Evaporation, spontaneous emulsification and phase separation process of Ouzo droplet in acoustic levitation.

Therefore, the next step is to estimate the concentration of each component in evaporating Ouzo droplets. Here we predict the concentration of ethanol, water, and anise oil components based on the experimental results. The mass fraction of each component can be obtained by equations (2) - (4).

$$Y_e = \frac{m_e}{m_e + m_w + m_A} \tag{2}$$

$$Y_w = \frac{m_w}{m_e + m_w + m_A} \tag{3}$$

$$Y_A = \frac{m_A}{m_e + m_w + m_A} \tag{4}$$

where Y is the mass fraction, e is ethanol, w is water, A is anise oil, and m is droplet mass. The masses shown here can be calculated by finding the theoretical droplet diameter by classical the droplet evaporation model (well-known d^2-law[7]). d^2-law can predict the droplet evaporation by considering the droplet mass transport by diffusion widely used in estimates of single droplet evaporation. d^2-law is expressed by equation (5).

$$d^2 = {d_0}^2 - \frac{8DM}{\rho_l R}\left(\frac{p_s}{T_s} - \frac{p_\infty}{T_\infty}\right)t \tag{5}$$

where M is molar mass, ρ_l is liquid density, R is gas constant, P is vapor pressure, T is temperature and t is time. This evaporation model was used to obtain the theoretical droplet diameter d_{th} as described in equations (6) and (7). With the theoretical droplet diameter, we can estimate the mass of the ethanol component in the evaporating droplet with equation (8).

$$d_{th} = \sqrt{{d_0}^2 - \beta t} \tag{6}$$

$$\beta = \frac{8DM}{\rho_l R}\left(\frac{p_s}{T_s} - \frac{p_\infty}{T_\infty}\right) \tag{7}$$

$$m_e = \frac{4}{3}\rho_e \pi \left(\frac{d_{th}}{2}\right)^3 \tag{8}$$

Meanwhile, the instantaneous droplet mass can be quantified from the experimental data with the equation (9). The mass of water and non-volatile anise oil was calculated by each volume obtained from the droplet diameter and each density as expressed by the equations (10) and (11, where V is droplet volume.. In acoustically levitated droplets, water vapor from the ambient air can condense on the droplet surface over time. As a result, the mass of the water in the evaporating droplet can be estimated by the difference between the experimental and theoretical diameters.

$$m_{exp} = \frac{4}{3}\rho_{exp} \pi \left(\frac{d}{2}\right)^3 \tag{9}$$

$$m_w = \left(m_{exp} - m_e\right) + \rho_w V_w \tag{10}$$

$$m_A = \rho_A V_A \tag{11}$$

Figure 6 shows the results of concentration estimation of Ouzo droplets with 70% ethanol concentration. **Figures 6 (a)-(c)** depict the time evolutions of normalized droplet surface area, the mass fraction in the droplet, and the droplet surface temperature. The highlighted area in **Figure 6 (b)** indicates the time at which the Ouzo effect occurred. In **Figure 6 (b),** the concentration of water rises over time. This is attributed to the condensation of surrounding water vapor as the ethanol evaporates. The surface temperature of the droplet interface plays a role in facilitating this water condensation. The droplet surface temperature was a few degrees colder than the ambient air, causing a temperature gradient that promotes condensation.

Onset condition of Ouzo effect and three-component phase diagram are shown in **Figure 7**. In **Figure 7 (a)**, the concentration of the anise oil was constant at 1%. In **Figure 7 (b)**, ○, △, □ represent the results for 1%, 5%, 10% anise oil. The results confirm that with an increase in anise oil concentration, the onset of the Ouzo effect was observed at higher ethanol concentrations. We used the three-component phase diagram to clarify the onset region of the Ouzo effect in acoustic levitation. In our future study, we aim to incorporate our experimental findings into this three-component phase diagram for a more systematic comparison and in-depth investigation.

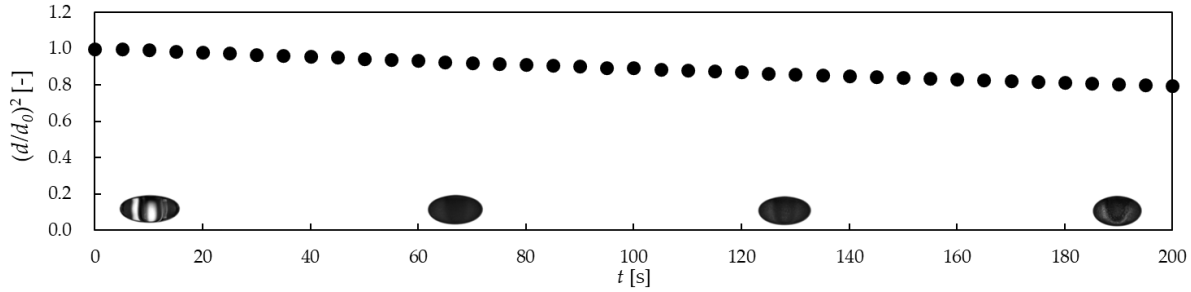

(a) Evaporation process

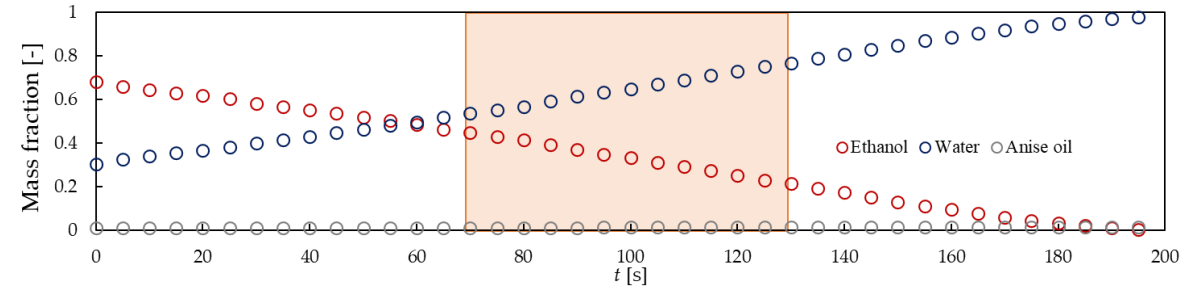

(b) Mass fraction in the droplet

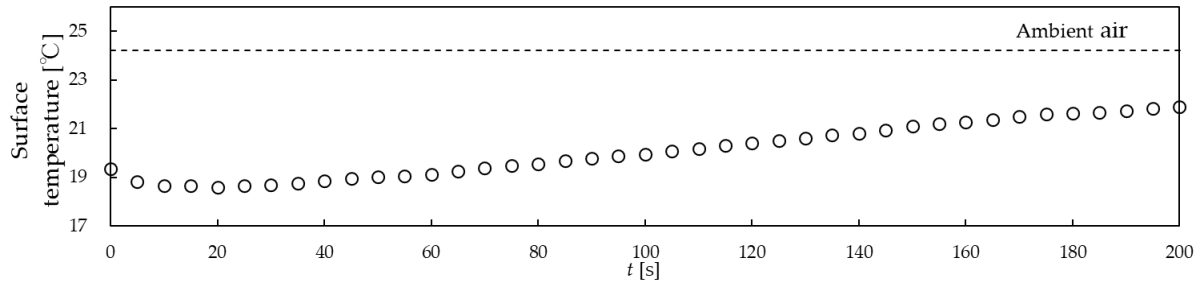

(c) Droplet surface temperature

Figure 6 Evaporation process, mass fraction, and surface temperatu of Ouzo droplet.

(ethanol: 70 vol%, water: 29 vol%, anise oil: 1 vol%)

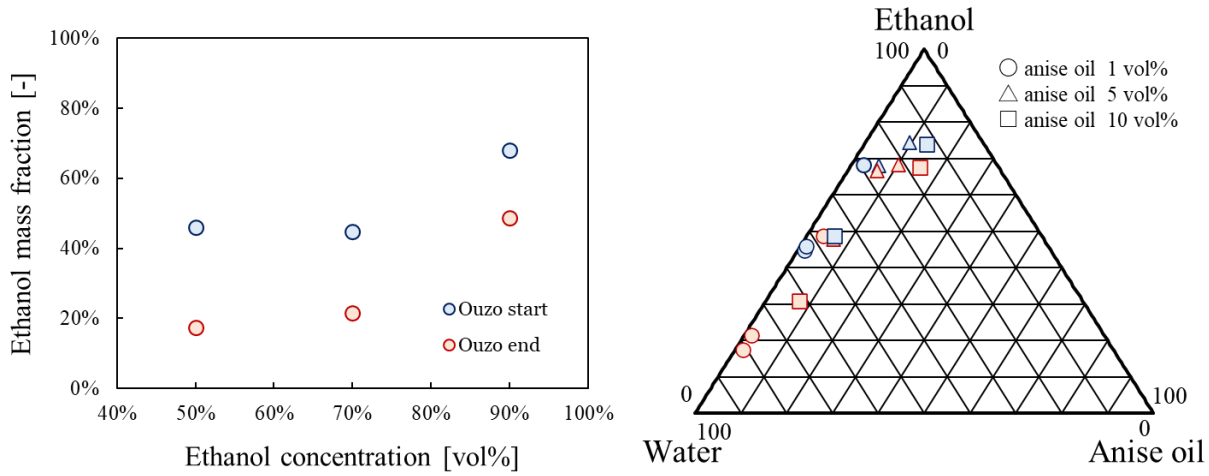

(a) Onset condition of Ouzo effect with different ethanol concentration (b) Phase diagram for Ouzo effect

Figure 7 Onset condition of Ouzo effect and three-component phase diagram.

4. Conclusions

The aim of this study is to understand the evaporation dynamics of spontaneous emulsification and phase separation associated with evaporation of Ouzo droplets. To achieve this, we visualized and quantified the spontaneous emulsification and phase separation processes using the droplet evaporation model. The obtained results are summarized as follows:

1) The Ouzo effect was observable even in a non-contact condition via an acoustic field.
2) The Ouzo effect occurred when the ethanol component ranged between 40% and 90%. It was also observed that a higher ethanol concentration delayed the onset of the Ouzo effect and reduced its duration.
3) Through experimental data, we explored evaporation, spontaneous emulsification, and phase separation of Ouzo droplets in an acoustic field, indicating a four-step process.
4) We were able to estimate the concentration of droplets at which the Ouzo effect occurs. The three-component phase diagram of water, ethanol, and anise oil was also created to show the region where the Ouzo effect occurs.

References

1) D. Foresti, M. Nabavi, M. Klingauf, A. Ferrari and D. Poulikakos: Proc. Natl. Acad. Sci. USA, 110, 31, (2013), 12549.
2) A. L. Yarin, M. Pfaffenlehner, C. Tropea: J. Fluid Mech., 359, (1998), 65.
3) Y. Abe, K. Hasegawa: JAS 69, 11, (2013), 591.
4) K. Hasegawa, K. Kono: AIP Adv., 9, (2019), 035313.
5) Y. Maruyama, K. Hasegawa: RSC Adv., 10, (2020), 1870.
6) H. Tan, C. Diddens, P. Lv, J. G. Kuerten, X. Zhang and D. Lohse: Proc. Natl. Acad. Sci., 113, 31, (2016), 8642.
7) A. Frohn, & N. Roth, Dynamics of droplets, Springer Science and Business Media, (2000).